Nickel ferrite nanoparticles for simultaneous use in magnetic resonance imaging and magnetic fluid hyperthermia

Evrim Umut[1],Mustafa Coşkun[2], Francesco Pineider[3], Debora Berti[4],Hakan Güngüneş[5]

[1]*Dokuz Eylul University,Department of Medical Imaging Techniques,İnciralti,35340, İzmir, Turkey*

[2]*Hacettepe University, Department of Physics Engineering, Beytepe, 06800, Ankara, Turkey*

[3]*Department of Chemistry and Industrial Chemistry, Università di Pisa and INSTM, Pisa, I-56124, Italy*

[4]*Department of Chemistry "U.Schiff", Università degli Studi di Firenze and CSGI, Sesto Fiorentino, I-50019, Italy*

[5]*Hitit University, Department of Physics, 19040, Çorum, Turkey*

We demonstrate MRI contrast enhancement and ac-field induced heating abilities of organically coated $NiFe_2O_4$ nanoparticles and discuss the underlying physical mechanisms involved in MRI and MFH. Structural characterization reveals that $NiFe_2O_4$ particles synthesized with a modified co-precipitation method have very narrow size distribution with 4.4 nm magnetic core and 15 nm hydrodynamic diameters, with relatively small fraction of agglomerates. The as-prepared particles present superparamagnetic behavior at room temperature, with ZFC–FC thermal irreversibility, blocking temperature and very small coercivity. *In vitro* hyperthermia experiments, performed in ac-field conditions under human tolerable limits, show that suspensions of synthesized nanoparticles exhibit a maximum SAR value of 11 W/g. ^{1}H-NMR relaxometry measurements indicate that suspensions of $NiFe_2O_4$ have a transverse-to-longitudinal relaxivity ratio r_2 / r_1 greater than two, as required for superparamagnetic MRI contrast agents. On the basis of the parameters obtained from magnetic measurements, by comparing the relevant theoretical models with experimental results we found that the presence of agglomerates and particularly the interactions within agglomerated nanoparticles has a significant effect on MFH and MRI efficiencies. On the other hand, from an applicative point of view, both MRI contrast enhancement and heating capabilities allow the simultaneous use of Ni-ferrites in diagnostic and therapeutic applications as theranostic agents.

I. INTRODUCTION

In the past decades, the biomedical use of magnetic nanoparticles became very popular as witnessed by the large number of publications introducing novel synthesis techniques, discussing the new application strategies and reporting the successful in vitro and in vivo application results, where actually the effectiveness in such biomedical applications mostly depends on the physiochemical and surface properties of nanoparticles. Among these applications magnetic resonance imaging (MRI), targeted drug delivery and magnetic hyperthermia are among the most promising ones. In MRI, which is a non-invasive technique for the diagnosis of diseases, magnetic nanoparticles are used as contrast enhancement agents [1-4], where the improved contrast in MR images permits better definition and precise locating of diseased tissues (e.g. tumors). On the other hand, in magnetic fluid hyperthermia (MFH), which is a thermal treatment of cancerous cells in conjugation with chemotherapy and radiotherapy, magnetic nanoparticles are used as heating mediators [5,6]. In this technique after intravenous injection of magnetic fluids into the body, nanoparticles are concentrated in the vicinity of malignant tissue either by site specific targeting or by the application

of an external magnetic field in action-at-a-distance manner. Localized particles are then exposed to a time-varying magnetic field and induce a temperature increase in the tissue, where increased temperature selectively kills cancerous cells which are more sensitive to relatively high temperatures [7]. In recent years considerable attention has been focused on multifunctional magnetic nanoparticles, in which the above mentioned diagnostic (MRI) and therapeutic (MFH) capabilities are combined together [8,9]. Such a possibility to combine the therapeutic effect generated by the heat release with the enhanced contrast in MRI is extremely appealing since it would provide the possibility to monitor the effect of the applied hyperthermia therapy.

Considering the biomedical applications of magnetic nanoparticles, as an alternative to iron oxides (Fe_3O_4 or γ-Fe_2O_3) which are the most studied materials among all ferrites due to its excellent biocompatibility, $NiFe_2O_4$ is a good candidate having reasonably high bulk saturation magnetization and low magnetic anisotropy. A proper surface coating can easily prevent toxic ion leakage from magnetic core to biological media and permits the use of $NiFe_2O_4$ nanoparticles in these applications. H. Yin et al. [10] have investigated the effect of particle size and surface coating on the cytotoxicity of $NiFe_2O_4$ and reported that $NiFe_2O_4$ nanoparticles encapsulated with an oleic acid coating as monomers exhibit no cytotoxic effect. Similarly, S. Rana et al. have shown that $NiFe_2O_4$ nanoparticles coated with polyvinyl alcohol, polyethylene oxide and polymethacrylic acid (PMAA) polymers, are well suited to be employed as magnetic carriers for drug delivery applications [11]. Several research groups have synthesized nickel ferrite nanoparticles with different physical methods, i.e. mechanical milling [12-14], thermal plasma vapor condensation [15], or through chemical techniques like sol-gel [16], co-precipitation [17-18], high temperature hydrothermal decomposition [19], microemulsion (micelle or reverse micelle) method [20]. Among these, the co-precipitation and hydrothermal decomposition methods seem to be the most suitable ones, since they allow synthesizing samples with high crystallinity, size-shape uniformity and enables in-situ or post-synthetic coating, which are the key requirements for biomedical applications. Despite remarkable attention in the literature, there are very few publications related to MRI or hyperthermia applications of surface coated nickel ferrite nanoparticles. M. Shultz et al. have prepared aqueous solutions of dopamine- and polyethylene glycol-functionalized nickel ferrite nanoparticles synthesized by reverse micelle method and investigated the MRI contrast enhancement abilities of synthesized samples by reporting the relaxometry measurement results together with MR test images [21]. On the other hand S. Bae and his colleagues [22], following the synthesis of uncoated and chitosan coated $NiFe_2O_4$ nanoparticles by sol-gel and thermal decomposition methods, have investigated ac magnetic field-induced heating properties of $NiFe_2O_4$ in solid state and in agar form. In another paper, [23] the same authors presented the hyperthermic characteristics of different sized $NiFe_2O_4$ particles for different applied magnetic fields and frequencies, and compared their hyperthermic efficiency with $CoFe_2O_4$ nanoparticles, a material with high magnetic anisotropy.

In this paper, we present a comprehensive study on organically coated monodisperse $NiFe_2O_4$ nanoparticles synthesized by a modified co-precipitation method. First, morphological, structural and surface characterizations of the synthesized nanoparticles are given. Thereafter, magnetic properties of nanoparticles in stable suspension form have been investigated, together with a discussion about the relation among such properties and the physical mechanisms underlying MRI and MFH applications. Regarding MFH efficiency of nanoparticle suspension, the self-heating temperature rise curves deduced for different biologically tolerable ac field conditions are presented and experimentally calculated specific absorption rate (SAR) values were compared with theoretical ones. Finally, MRI contrast enhancement ability of magnetic fluid prepared with nanoparticles is investigated by means of nuclear magnetic relaxation dispersion (NMRD) profiles, where a theoretical fitting of this profile with known model for superparamagnetic proton relaxation is also given. As a result, the synthesized

monodisperse $NiFe_2O_4$ nanoparticles, which form a very stable suspension in carrier liquid, showed both MRI contrast increment and heating effect and can serve both as MRI contrast agents and hyperthermia mediators at the same time. To the best of our knowledge, this is the first study reporting this simultaneous application potential of nickel ferrite nanoparticles with a narrow size distribution for MRI and MFH.

II. EXPERIMENTAL

A. Synthesis of organically coated $NiFe_2O_4$ nanoparticles and preparation of their stable dispersion

Nanoparticles were prepared with a synthesis method introduced by Caruntu et al. [24], which is based on the decomposition of metallic precursors in liquid phase environment. In this three-step synthesis method, following the formation of metal compounds, the hydrolysis/condensation of these materials is realized at second step and finally the particles are coated with oleic acid. All chemicals and solvents used in the synthesis were purchased from Sigma-Aldrich and Alfa Aesar Chemical Company and used as received without further purification. Briefly, after dissolving 10 mmol $FeCl_3 \cdot 6H_2O$ in 175 ml diethylene glycol in a three neck flask, 5 mmol $NiCl_2 \cdot 6H_2O$ is added to the solution and mixed for 1 hour with magnetic stirrer at maximum speed. An individually prepared mixture of 40 mmol NaOH with 80 ml diethylene glycol was injected to the solution and this solution was mixed for 4 hours under N_2 flow, while a gradual change of mixture color from yellow to brown was observed during this process. Thereafter, the mixture was heated to 210 ^oC and maintained at this temperature for 2 hours, while 55 ml of diethylene glycol including 8 mmol of oleic acid were added. After cooling down to room temperature, the mixture was then centrifuged at 4000 rpm for 20 min and nanoparticles were obtained as a precipitate. After washing the precipitate with methanol and dispersing in toluene, as a size selection process, relatively larger particles were isolated from sample by subsequent precipitation, redispersing and centrifugation. Finally, the particles were stabilized with tetramethyl ammonium hydroxide (TMAH), which also works as a solvent, and then transferred to aqueous phase. The particle dispersion in water exhibits excellent stability for very long time period even under strong magnetic field.

B. Structural characterization via XRD, TEM, DLS, FTIR

X-ray diffraction (XRD) pattern of nanoparticle powder was collected by using a Rigaku D/Max-Ultima diffractometer (having Bragg-Brentano geometry) equipped with a divergence slit of 1^o, anti-scatter slit of 1^o and detector slit of 0.3 mm. Sample was scanned with Cu-Kα radiation obtained under 40 kV/40 mA, where the scanning performed with 0.02^o angular steps and four times slower than normal speed. Standard resolution and high resolution Transmission Electron Microscopy (TEM and HRTEM) images of nanoparticles were obtained with JEOL JEM-2100F, which is a field-emission sourced scanning transmission electron microscope (STEM) with highest 0.19 nm point resolution. The sample was prepared for analysis by dispersing the nanoparticle powder in ethanol and by depositing a drop of such dispersion on a copper-carbon grid. The images were obtained in bright field mode with acceleration voltage of 200 kV. Dynamic Light Scattering (DLS) measurements were performed with a Brookhaven Instruments 90Plus Nanoparticle Size Analyzer. The light scattered from the sample was collected at 90° with respect to the incident 659 nm laser light radiation. The obtained autocorrelation function cannot be fitted with the cumulant method, highlighting the multimodality of the sample, and was therefore Laplace-inverted with CONTIN [25] algorithm. The size distribution was evaluated in terms of intensity-weighted diameters. Infrared absorption spectra were recorded with a Perkin Elmer One Fourier transform infrared (FTIR) spectrometer, equipped with a deuterated triglycine sulfate (DTGS) detector and can scan a wavenumber range between 400 and 4000 cm^{-1}. Prior to the analysis a KBr pellet, including

coated $NiFe_2O_4$ powder as 1:100 mass ratio, was prepared. The spectra of this sample was then subtracted from the background spectra of pure KBr sample.

C. Magnetometry measurements with SQUID

Magnetic measurements were carried out on powders and suspension of nanoparticles using a Quantum Design Superconducting Quantum Interference Device (SQUID) MPMS magnetometer. In order to obtain zero field cooling (ZFC) curves, after cooling down the sample to lowest temperature (5 K) in the absence of any magnetic field, the magnetic moment has been measured under a static field of 100 Oe by slowly heating the sample to 300 K. For field cooling (FC) curves, the temperature was decreased back to 5 K, without removing the dc magnetic field. For obtaining the hysteresis curves, magnetic field has been swept between ±5 T both at 5 K and at 300 K.

D. Relaxometry measurements on nanoparticle suspensions

In order to obtain Nuclear Magnetic Relaxation Dispersion (NMRD) profiles of nanoparticles suspension, as a measure of their MRI contrast increasing capability at different frequencies, the longitudinal (T_1) and transverse (T_2) relaxation times of ^1H nuclei has been measured by varying the magnetic field, in the Larmor frequency range 10kHz - 300 MHz. The measurements were performed at room temperature, but differences between the results measured at room and physiological temperatures were normally within 10%. Proton NMR signal has been collected with two different pulsed FT NMR spectrometers: i) a fast-field cycling Stelar SMARTracer (10kHz – 10MHz range) and ii) an Apollo Tecmag (for ν >10 MHz). The longitudinal and transverse relaxation times, T_1 and T_2, have been measured by performing standard saturation recovery and Carr-Purcell-Meiboom-Gill (CPMG) pulse sequences, respectively.

E. Time-dependent calorimetric measurements on nanoparticle suspensions

Hyperthermia efficiency of the nanoparticle suspension, , has been investigated by recording the temperature change of the magnetic fluid under ac magnetic field. The measurements were carried out on a specially designed homemade setup consisting of an Ambrell Easyheat-LI rf power supply (power: 4,2–10 kW, frequency: 150-400 kHz), a helical coil (90 turns, inner diameter: 6.35 cm) wound around the tube holder, a fiber thermometer connected with a LabView-controlled digital multimeter and a computer. All the heat losses from magnetic fluid-containing tube have been minimized with specific arrangements for reaching an adiabatic condition. Time dependent temperature rise was recorded at constant frequency of f=170 kHz, by changing field amplitudes between 17.2 and 23.7 kA/m, these field parameters being within human body tolerable limits.

III. RESULTS AND DISCUSSION

A. Structural properties

The x-ray powder diffraction pattern (XRPD) of the synthesized sample is given in Fig.1. Indexing of the observed diffraction peaks indicates that the as-prepared particles have cubic spinel crystal structure. The lattice constant a for each peak was calculated by using the formula for cubic crystals: $a = (h^2 + k^2 + l^2)^{1/2}$, where d is the interplanar spacing and h, k, l are miller indices of the crystal planes. The mean lattice constant a_0 was determined to be 8.36 Å, a result in agreement with the reported value for $NiFe_2O_4$ in JCPDS cards file No.10-0325. The broadening of the peaks in the pattern is due to the small size of the crystallites and the mean crystallite size D of particles can be calculated by using the Debye-Scherrer formalism: $D = 0.9\lambda/\beta cos\theta$, where λ is the wavelength of Cu-Kα radiation, β is the full width at half maximum (FWHM) intensity of the broadened peak and θ is the Bragg angle at which the diffraction peak is observed. By applying this formula to the most intense (311) peak and using the FWHM value obtained from Gaussian fit of this peak, the mean diameter for $NiFe_2O_4$ nanocrystals was found to be 4.43 nm. Mean crystallite size values calculated from other diffraction peaks, together with other XRD experimental data are given in Table.1.

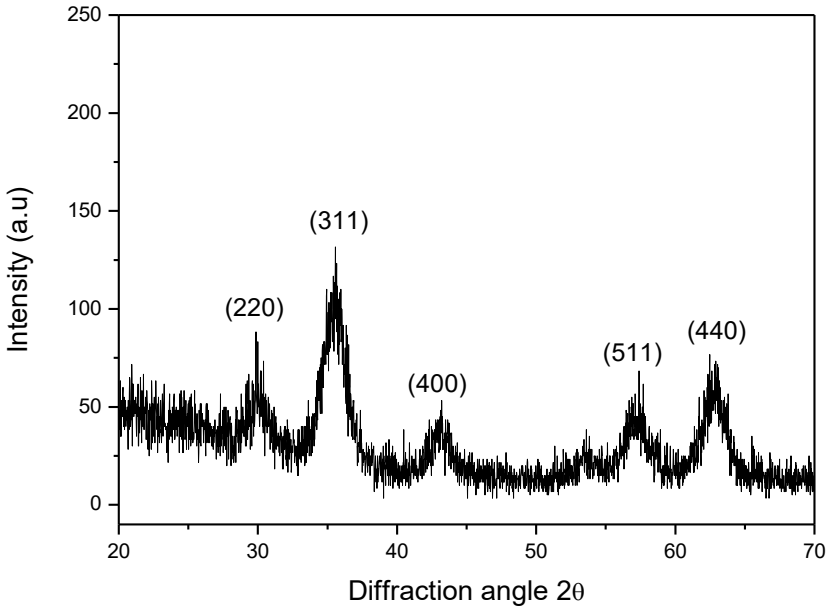

Fig.1. X-ray powder diffraction (XRPD) pattern of as prepared $NiFe_2O_4$ nanoparticles

Table.1. XRD data and calculated values of lattice constant a_o and nanocrystal size D for each diffraction peak

2θ (°)	d (Å)	FWHM (°)	h k l	a_0 (Å)	D (nm)
30,00	2,975	1,738	(220)	8,41	4,78
35,57	2,521	1,888	(311)	8,36	4,43
43,26	2,089	1,699	(400)	8,36	5,03
57,39	1,604	1,902	(511)	8,34	4,78
63,04	1,473	1,801	(440)	8,33	5,15

The morphology of the synthesized $NiFe_2O_4$ nanoparticles has been investigated by TEM images. Normal resolution TEM image (Fig.2a), shows that particles have uniform spherical shapes and generally stand well apart each other; this is most probably ensured by the oleic acid and TMAH coating on their surface, which cannot be observed (due to its low molecular

weight) in TEM. However, there are also agglomerates which can be seen in TEM images (inset of Fig2a). In Fig.2b, a histogram graph of the particle size distribution, determined by statistically analyzing more than 300 particles in the image with a digital image processing program (Image-J), is shown. This histogram data were fitted with log-normal function and the average size of the particles is calculated as 4.41 ±0.02 nm, in good agreement with XRD results. On the other hand, the high resolution HRTEM image given in Fig.2c shows the crystal nature of the particles (uniform contrast) and the distance between adjacent lattice planes can be measured (inset of Fig.2c). More evidence on the crystal nature of the particles and the alignments of the nanocrystals can be obtained by looking at the selected area electron diffraction pattern (SAED) corresponding to the HRTEM image (Fig.2d). In SAED pattern, considering that each pair of equal-radial distant spots represents diffraction from one crystal plane at certain orientation, the diffraction circle of (311) planes indicates that nanoparticle ensemble is mostly constituted by randomly oriented single crystals. Identification of other diffraction spots as (220), (400), (440) and (511) confirms the cubic spinel structure of particles, coherently with XRD data.

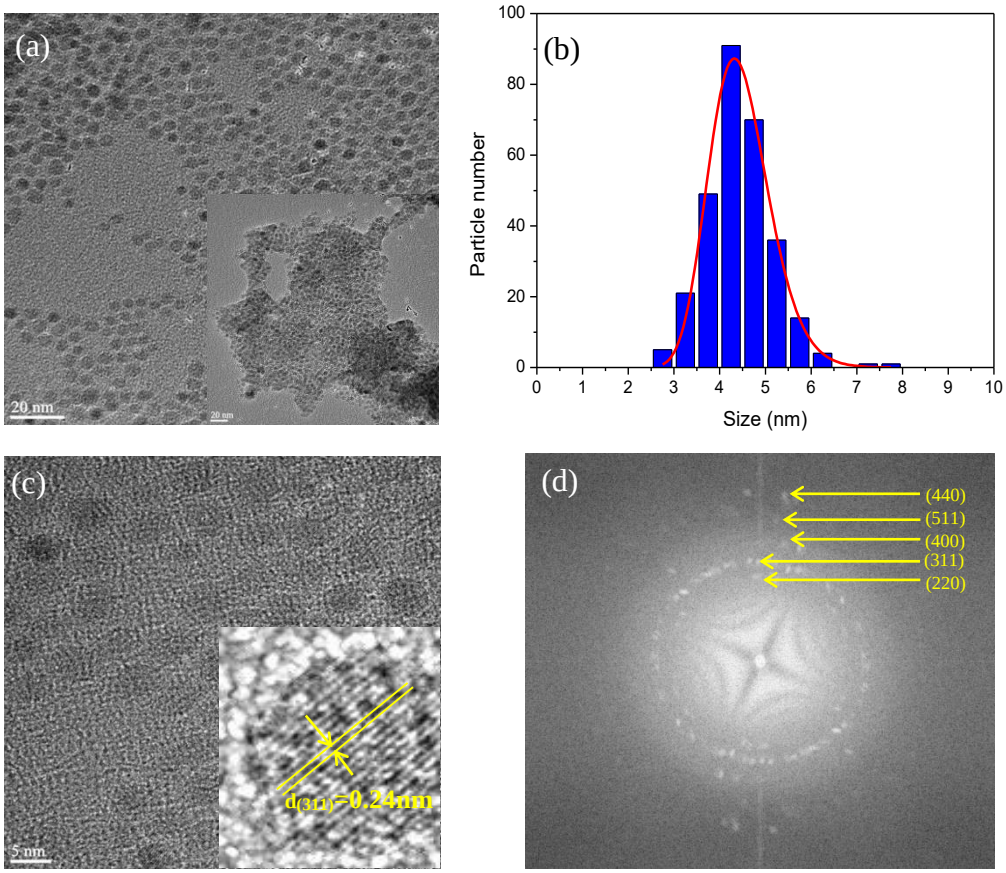

Fig.2. TEM images (a), size distribution histogram (b), HRTEM images (c) and SAED pattern (d) of $NiFe_2O_4$ nanocrystals.

TEM measurements do not supply information on particles' hydrodynamic size. For this reason Dynamic Light Scattering (DLS) measurements have been performed, where the volume-size and the number-size distributions have been obtained from the intensity-weighted distribution, inserting the real and imaginary parts of the refractive index of $NiFe_2O_4$ particles [26]. DLS

results (presented in supporting information-S1) reveal three different size populations: a dominant population of small particles with diameters around 15 nm, an intermediate one, whose size ranges around 100 nm and a larger one, characterized by sizes around 1 μm, where the relative abundance of latter two populations is very low. Clearly, the first population belongs to isolated nanoparticles observed in TEM and the hydrodynamic size, larger than obtained by TEM, means that nanoparticles were successfully coated. However the second and third populations are a signature of the presence of aggregates of primary particles, even though with low relative abundance.

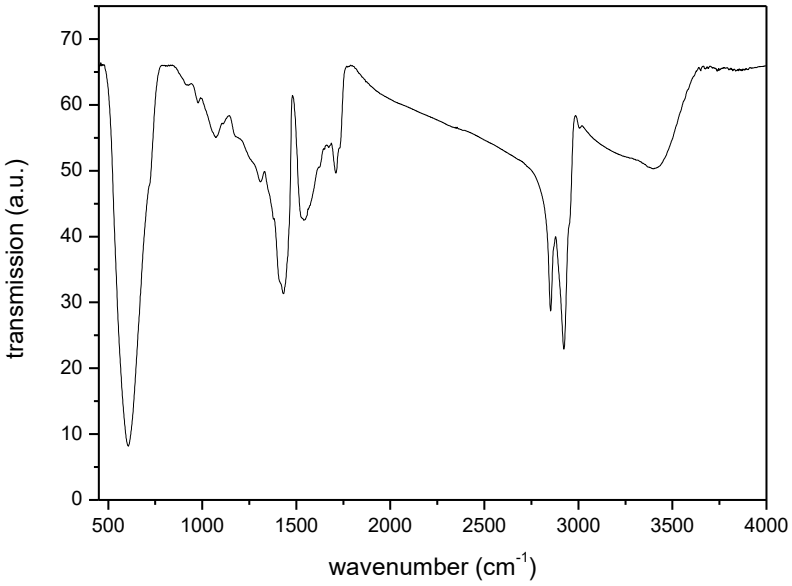

Fig.3. FTIR spectrum of oleic acid and TMAH coated NiFe2O4 nanoparticles in powder form.

The presence of oleic acid and TMAH molecules on the surface of $NiFe_2O_4$ nanoparticles has been further confirmed by Fourier Transform Infrared (FTIR) spectroscopy. Fig.3 shows the infrared transmission spectra of coated nanoparticles in powder form. The broad peak around 3400 cm^{-1} characterizes O-H vibrations of the hydroxyl group present in TMAH molecule. The sharp peaks observed at 2923 cm^{-1} and 2852 cm^{-1} can be associated with asymmetric and symmetric C-H stretching of the long CH_2 chain in oleic acid and CH_3 groups in TMAH, respectively. The other two close peaks at 1544 cm^{-1} and 1431 cm^{-1} are attributed to the stretching vibrations of COO^- and a superimposed small peak at 1710 cm^{-1} represent C=O stretching; this result clearly shows that oleic acid molecules are successfully coated around $NiFe_2O_4$ surface [27]. Furthermore, the strongest absorption peak observed in the spectra at 604 cm^{-1} is related with the $NiFe_2O_4$ magnetic core and corresponds to the stretching vibrations of metal-oxygen bonds in the tetrahedral sites of the spinel structure, whereas the characteristic IR absorption peak of metal-oxygen bonds in octahedral sites (expected around 405 cm^{-1}) cannot be observed since it is unfortunately out of the scan range of our spectrometer.

B. Magnetic properties

Magnetic behavior of synthesized $NiFe_2O_4$ nanoparticles was investigated by means of temperature and field dependent magnetization measurements. The zero field and field cooling (ZFC-FC) curves shown for powder sample in Fig.4a represent the typical behavior of an ensemble of single domain superparamagnetic nanoparticles with the critical temperatures of irreversibility (i.e. the temperature at which the ZFC and FC curves split) T_{irr} ~ 110 K, and the temperature of ZFC maximum T_{max}~ 12 K. The superparamagnetism implies a thermally activated reversal phenomenon for the magnetic moments of the particles so-called as Néel relaxation [28,29], where the Néel reversal time τ_N is given by Arrhenius law:

$$\tau_N = \tau_0 \exp\left(\frac{K_{eff}V}{k_BT}\right) \quad (1)$$

where τ_0 is the attempt time, whereas k_BT is the thermal energy and $K_{eff}V$ is the magnetic anisotropy energy barrier, given by the product of the effective anisotropy constant K_{eff} and the magnetic core volume V. According to Eq.1, when the condition $(2\pi/t_m)\cdot\tau_N \sim 1$ is fulfilled, i.e. the measuring time t_m is close to the order of the moment fluctuations, the system appears blocked. On this respect, T_{irr} in ZFC-FC curve corresponds to the magnetization blocking of the largest particles (having biggest energy barrier) in the size distribution, whereas T_{max} can be associated with the blocking of the mean sized particles, which comprise the majority of the particle ensemble. For this reason, T_{max} can be assumed as the blocking temperature of the system.

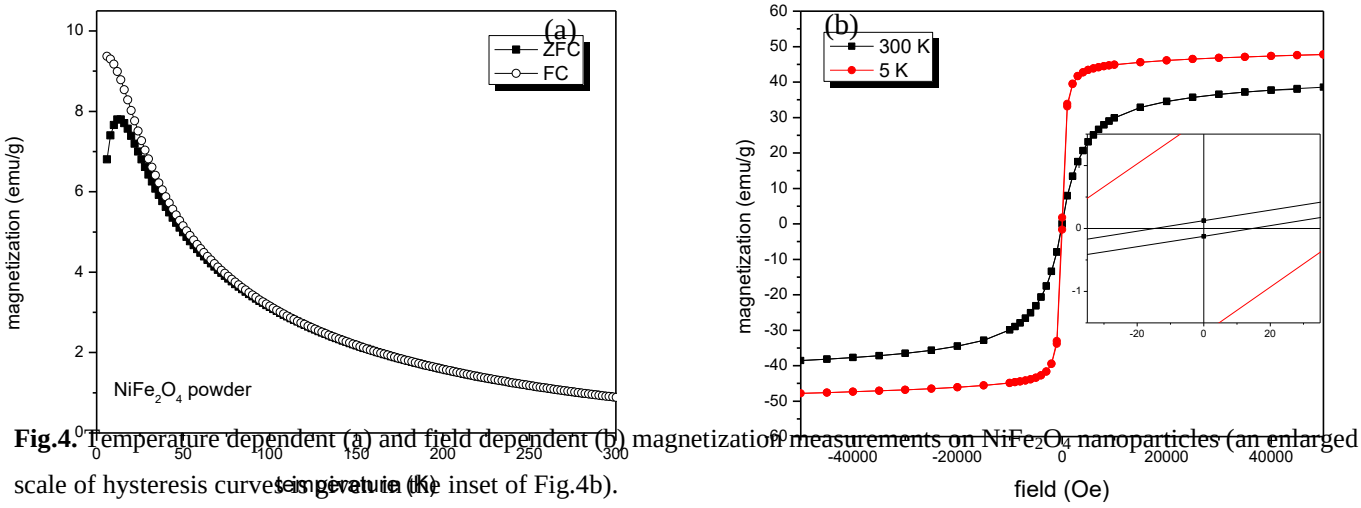

Fig.4. Temperature dependent (a) and field dependent (b) magnetization measurements on $NiFe_2O_4$ nanoparticles (an enlarged scale of hysteresis curves is given in the inset of Fig.4b).

At the blocking temperature T_B, by substituting typical values of t_m=1 s for standard dc magnetometry measurements and τ_0=10^{-9} s for non-interacting or weakly interacting particles, Eq.1 reduces to $T_B \cong K_{eff}V/21k_B$. Hence as a first approximation, assuming monodispersed spherical nanoparticles and using the particle volume calculated with the mean size value obtained from TEM, the magnetic anisotropy constant K_{eff} of the synthesized $NiFe_2O_4$ nanoparticles takes the value K_{eff}=0.79x10^6 erg/cm^3. This value of K_{eff}, which is the total anisotropy energy density including the magneto-crystalline, surface and shape anisotropy contributions, is much greater than the reported value of 0.07x10^6 erg/cm^3 for bulk $NiFe_2O_4$ [30], as expected for such small nanoparticles where the surface anisotropy contribution is quite high due to enhanced surface to volume ratio.

In the field dependent magnetization measurements shown in Fig.4b, an open hysteresis curve with a coercive field H_c=98 Oe is observed at T=5K, whereas the M(H) curve at room temperature shows a closed hysteresis loop, which means that the

nanoparticles are unblocked at room temperature. Nevertheless, the small coercive field (H_c=30 Oe) observed at room temperature indicates that some particles, probably the larger agglomerates detected in DLS measurements, are in the blocked state. Both M(H) curves in Fig.4b do not reach the saturation even at the highest magnetic field of H=5 kOe. However, the saturation magnetization M_s can be estimated by fitting the magnetization data at high magnetic fields to the empirical formula $M = M_S + b/H + c/H^2$. By this method the saturation magnetization of the nanoparticle powder has been calculated as M_s=40.8 emu/g at room temperature, which is smaller than the reported value of M_s=55 emu/g for bulk $NiFe_2O_4$. This difference, as consistent with calculated anisotropy value, is a consequence of the disordered spin layer at the surface of nanoparticles, which do not contribute to the particle magnetization. Such disorder can have different origins: i) spin canting due to the minimization of magneto-static energy at the surface and/or ii) spin-glass like behavior due to the broken exchange bonds or formation of chemical bonds between coating molecules and surface metal ions [31]. Discrimination between these two effects (finite size effect and coating effect) is rather difficult.

The M (H) curve (Fig.4b) of a superparamagnetic nanoparticle ensemble obeys the Langevin function:

$$L(x) = \coth(x) - \frac{1}{x} \tag{2}$$

where $x = M_S VH/k_B T$ and $M_S V$ is the magnetic moment of each particle with V being the volume of the particles magnetic core. Assuming spherical nanoparticles, by fitting the $M(H) = M_S L(x)$ function to the room temperature M-H curve (see supporting information-S2), the mean diameter of the particle has been calculated as d=4.6 nm, which is in good agreement with values obtained by TEM and XRD.

For magnetic nanoparticles suspended in a carrier liquid (ferrofluid), in addition to Neel relaxation the particle moments can change direction with Brownian relaxation, which is described as the rotation of the particle as a whole in the liquid environment. The relaxation time due to the Brownian rotation τ_B(Eq.3) is given by Stokes-Einstein equation for spherical particles, where η is the viscosity of the carrier liquid and $V_h$the hydrodynamic volume of nanoparticles:

$$\tau_B = \frac{3\eta V_h}{k_B T} \tag{3}$$

Hence by using the hydrodynamic diameter (15 nm) deduced from DLS measurements and the viscosity of water at the melting point (η=1,8x10^{-3} N.s.m^{-2}), the relaxation time value τ_B becomes around one microsecond, whereas the calculated Néel relaxation time τ_N at the same temperature according to Eq.1 falls in the
nanosecond scale. In other words, when an effective relaxation rate for the magnetic moments of nanoparticles is defined as

$$\frac{1}{\tau_{eff}} = \frac{1}{\tau_N} + \frac{1}{\tau_B} \tag{4}$$

one can conclude that the Brownian relaxation is too slow as compared to Neel relaxation, which means that the Neel reversal of magnetization is the mechanism primarily responsible for magnetic relaxation of the prepared ferrofluid.

C. Hyperthermia measurements

When magnetic nanoparticles are subjected to an ac magnetic field with suitable frequency and amplitude, energy is converted to heat released in the surrounding medium through hysteresis losses and the above mentioned Neel and Brownian mechanisms [32]. The heating capacity of a ferrofluid is quantified by means of the specific absorption rate (SAR), also known as specific loss of power (SLP), which is defined as the amount of heat power released per mass of magnetic nanoparticle. One common method to determine the SAR value is to investigate the ac field-induced temperature rise of the ferrofluid in a given time interval. Fig.5 shows the experimental results of such calorimetric measurements performed on the prepared $NiFe_2O_4$ nanoparticle suspension. In these measurements alternating field frequency f was kept constant at f= 170 kHz and the field amplitude H_o varied between 17.2 and 23.7 kA/m, which corresponds to a maximum product value of $H_o f = 4.0 \times 10^9$ A·m^{-1}·s^{-1}.

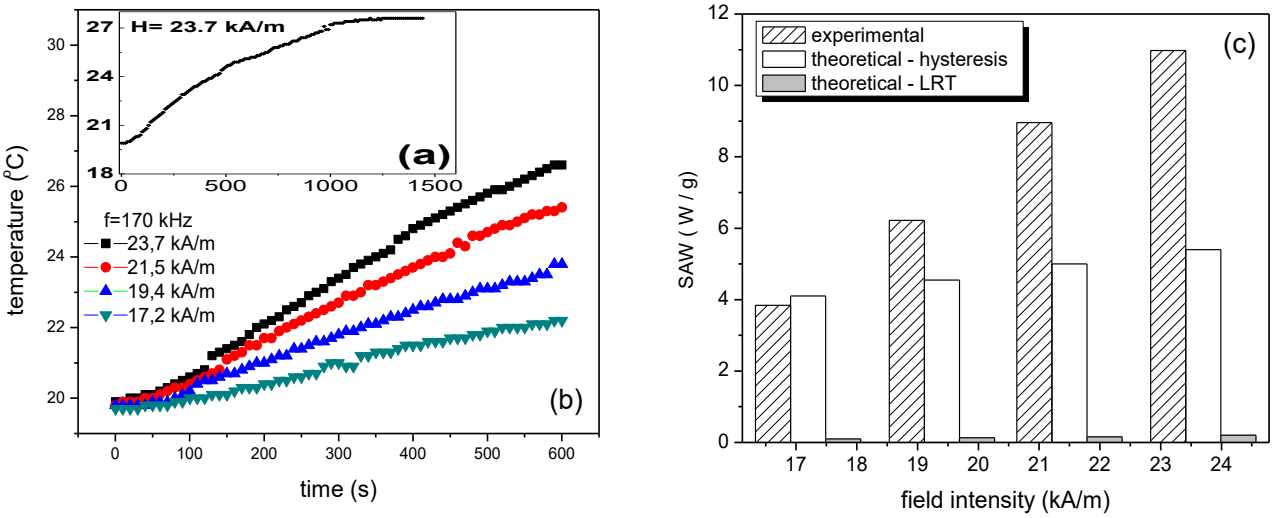

Fig.5. (a) ac field-induced temperature rise curves of $NiFe_2O_4$ suspensions in long (inset) and short (main graph) time range. (b) Experimentally deduced SAR values in comparison with theoretical values calculated by Eq.6 and Eq.7.

This value is under the threshold limit (5×10^9 A·m^{-1}·s^{-1}) estimated by Hergt et al. [33] for a small exposed region in human body, which means that these field parameters can be safely applied for small-area local treatment purposes. On the other hand, since the inducing eddy current power is proportional with $(H_o \cdot f \cdot d)^2$ where d is the current loop diameter, using the same field parameters in relatively larger areas may cause unwanted physiological responses i.e. possible cardiac and arrhythmia stimulations due to the variation of bioelectricity, stimulation of skeletal muscle and serious brain or cranial nerve damage [34]. For example Brezovich et al.[35], after their experiments on human patients, reported that for a loop diameter of d≈30 cm a value of $H_o f = 4.85 \times 10^8$ A·m^{-1}·s^{-1} should not be exceeded.

In the inset of Fig.5a one observes that by applying the maximum field intensity the temperature increases in time until reaching a maximum temperature difference ΔT_{max}=7 °C (in 20 min) from starting temperature of 19 °C, meaning that when extrapolated to physiological temperatures, the desired hyperthermia temperature values (40-42 °C) for selective cell damage could be attained. Another observation in the inset of Fig.5a is that the temperature rising rate decreases with increasing temperature and time as generally observed in in-vitro magnetic fluid hyperthermia experiments. This behavior can have several physical reasons such as: i) thermal degradation of magnetic spin structure (hence magnetic moment) of nanoparticle effecting the heat generation through Néel relaxation process; ii) temperature induced viscosity variation of carrier liquid which may change the "Brownian rotation" contribution to heat generation [22]; iii) an increasing heat exchange depending on the temperature

difference between magnetic fluid and its surrounding due to the fact that the experimental setup is not perfectly adiabatic. On the other hand, as shown in the main graph of Fig.5a, the initial part of the temperature rise curves for all applied fields are roughly linear and, by taking the initial slope d*T*/d*t* of the curves, the calculation of SAR is possible using the equation:

$$SAR = \frac{\sum_i c_i m_i}{m_{NP}} \left(\frac{dT}{dt}\right) \tag{5}$$

In Eq.5 the heat capacity of the sample, which is the sum of the heat capacity of each constituent $c_i m_i$ in the magnetic fluid, is divided by the mass of the magnetic nanoparticles m_{NP}. Since the $NiFe_2O_4$ nanoparticle concentration is low (~4.5 mg/mL) in the suspension, in our calculation the heat capacity of water (4.18 J/g°C) was taken as the sample's heat capacity and the initial slope was determined from a linear fit of the temperature rise curves. Fig.5c shows experimentally obtained SAR values with Eq.5, where strong dependence of these values (11 W/g for 23.7 kA/m) from the field intensity is observed. In particular, according to linear response theory (LRT) [36], the heating power produced by magnetic fluids is proportional to frequency *f* and the square amplitude H_o^2 of excitation field. Since the magneto-thermal energy conversion originates from the delay of particle moment relaxation (either by Néel or Brownian processes) with respect to oscillating ac magnetic field, the heat power dissipation is also proportional to out-of-phase component of ac magnetic susceptibility χ''. Therefore, as supposed by Rosenweig [37], for magnetic fluids including superparamagnetic nanoparticles, a theoretical description of SAR can be given by

$$SAR = \frac{P}{\rho} = \frac{\mu_0 \pi}{\rho} f H_0^2 \chi'' \tag{6}$$

where *P* is the volumetric power dissipation, ρ is the mass density and μ_0 is the magnetic permeability of vacuum. In Eq.6 the imaginary part of ac susceptibility χ'', whose value at working frequency (f=170 kHz) cannot be directly measured by commercial magnetometers, can be written as $\chi'' = \chi_0 2\pi f \tau_{eff} / \left[1 + \left(2\pi f \tau_{eff}\right)^2\right]$ where τ_{eff} is the effective relaxation time given by Eq.4 and χ_o is the static susceptibility, which as a good approximation equals to $\chi_0 \approx \mu_0 M_s^2 V / k_B T$. Substituting these into Eq.6, one obtains:

$$SAR = \frac{\pi f V (\mu_0 M_s H_0)^2}{\rho k_B T} \frac{2\pi f \tau_{eff}}{1 + \left(2\pi f \tau_{eff}\right)^2} \tag{7}$$

The second term in Eq.7 has a strong dependence on particle size due to τ_{eff} (Eq.4, Fig.6b-inset) and for correct estimation of SAR, the size distribution of nanoparticle ensemble should be considered. For this reason, by taking into account the log-normal size distribution deduced by TEM and using parameters from structural and magnetic characterization ($d_h \cong d+10$nm, M_S=40.8 $A \cdot m^2 \cdot kg^{-1}$, $K_{eff}=0.77 \times 10^5$ $J.m^{-3}$, $\tau_0=10^{-9}$), theoretical SAR values has been calculated with Eq.6 for experimental conditions *f*=170 kHz and H_0=17.2-23.7 kA/m. As depicted in Fig.5b, calculated values (in solid columns) are very small compared to experimental ones (dashed columns). In fact, when the characteristic time of hyperthermia experiment is considered, with same parameters Eq.6 predicts a maximum SAR value of 202 W/g for the condition $2\pi f \tau_{eff} \approx 1$, which is fulfilled when the mean particle size equals to d≅9.2 nm. However, for particles with sizes d < 9.2 nm, Néel reversal of magnetization always dominates to Brownian rotation which leads to $\tau_{eff} \cong \tau_N$ and a very sharp decrease in SAR with

decreasing particle size is observed (Figure.6a,c). Eventually, for our $NiFe_2O_4$ particles in suspension (d_{mean}= 4.4 nm) since $2\pi f \tau_{eff} \ll 1$, very small SAR values (0,1-0,2 W/g) are obtained. When normalized to field parameters (dividing by $f.H_o^2$), similar SAR values have been experimentally observed in the literature for $NiFe_2O_4$ particles having very similar size distribution [38].

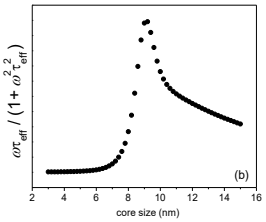

Fig.6. a) Size dependence of relaxation times (τ_N, τ_B, τ_{eff}) assuming parameters K_{eff}=0,77x10^5 J/m^3, τ_0=10^{-9}s, η=10^{-3} N.s.m^2 d_H = d + 10nm b) Calculated values of the second term in Eq.7 c) Size dependence of the calculated SAR values according to linear response theory.

The significant discrepancy between experimental and theoretical SAR values implies that Eq.6 based on the LRT is not enough to completely explain the experimentally observed SAR and hysteresis losses should be involved in heat generation. As evidenced by DLS measurements, despite of their weak abundance, larger agglomerates of $NiFe_2O_4$ nanoparticles coexist with isolated single-domain superparamagnetic particles in the suspension and those particles forming the agglomerates have different relaxation dynamics with respect to isolated ones, due to effective dipolar and/or exchange interactions among them. In particular, interparticle interactions give rise to an increase in anisotropy energy barrier and average blocking temperature of nanoparticles, which means that the agglomerated particles may still be in blocked regime and show ferromagnetic property at temperatures and frequency of hyperthermia experiment. The small hysteresis obtained with quasi-static magnetization measurements (see Fig.4b) is an indication of these agglomerates in blocked regime and in this case the SAR can be simply calculated from the area under the hysteresis curve as:

$$SAR = \mu_o f \int_{-H_o}^{H_o} M_{(H)} dH \qquad (8)$$

The SAR values extracted from hysteresis area (hollow columns in Fig. 5c) obtained with quasi-static measurements are nearly one order of magnitude greater than values anticipated by LRT, but are still smaller than experimental ones. However, certainly one should expect larger area in dynamic hysteresis curve measured at the frequency of hyperthermia experiment (f=170 kHz), and a better consistency with experimental SAR, which is always underestimated due to non-adiabatic experimental conditions. In this respect, we can conclude that agglomerated nanoparticles primarily contribute to the heat generation in the suspension.

In summary, in addition to structural and magnetic characteristics of nanoparticles like the mean size, size distribution, and magnetic anisotropy, dipolar interactions between particles also play determining role in the heat production, and similar observations have been reported in a considerable number of papers[39-43,]. In fact, in order to achieve the highest SAR values with magnetic nanoparticles, rather than almost concluded discussions on optimal size and material, the role of dipolar interactions is still under investigation. Recently, there was significant effort to develop theoretical models describing the influence of dipolar interactions on hyperthermia properties [44-49]. In these models performed with different numerical simulations, it is predicted that dipolar interactions have a significant effect on the SAR, being capable of both decreasing and increasing it, depending on the external field parameters and particle anisotropy. In particular, it is found that for soft magnetic particles, SAR can be increased by orders of magnitude with dipolar interactions, consistently with our observation. In contrast, for hard magnetic particles having relatively high magnetic anisotropy, the efficacy of heat release is hampered by dipolar interactions.

D. Relaxometric measurements

Superparamagnetic nanoparticles serve as MRI contrast improving agents, where the image contrast depends mainly on proton density, longitudinal (T_1) and transverse (T_2) nuclear relaxation times differently weighted along different parts of the body. Under the external magnetic field used in MRI, magnetized nanoparticles create inhomogeneous local fields on nearby protons and the time evolution of these dipolar fields is at the origin of the contrast enhancement effect. In particular, fluctuating fields generated by the electronic spins of nanoparticles, interacting with the nuclear moments of protons, cause the shortening of the nuclear relaxation times T_1 and T_2, thus modifying the local MRI signal intensity. Superparamagnetic nanoparticles effectively decrease T_2 at a greater extent than T_1; hence, they are used as T_2-relaxing (or negative) contrast agents, giving images with darker regions where they are delivered. Contrast enhancement capabilities of superparamagnetic fluids are evaluated by means of the relaxivities $r_{1,2}$, which are defined as the increment in proton relaxation induced by one mmol of magnetic ion per liter: $r_{1,2} = \left[\left(1/T_{1,2}\right)_{sup} - \left(1/T_{1,2}\right)_{dia}\right]/C$ where C is the molar concentration of magnetic ions. A conventional method to test the contrast improving ability of nanoparticles is to measure the longitudinal and transverse relaxivity as a function of proton Larmor frequency (i.e. the applied magnetic field), known as nuclear magnetic relaxation dispersion (NMRD) curves. Fig.7 presents the NMRD profiles of $NiFe_2O_4$ nanoparticles dispersed in water, where the longitudinal relaxivity r_1 exhibits a behavior typical of superparamagnetic dispersion in liquid: it remains flat at low frequencies, then reaches to a maximum and finally decreases rapidly at high frequencies.

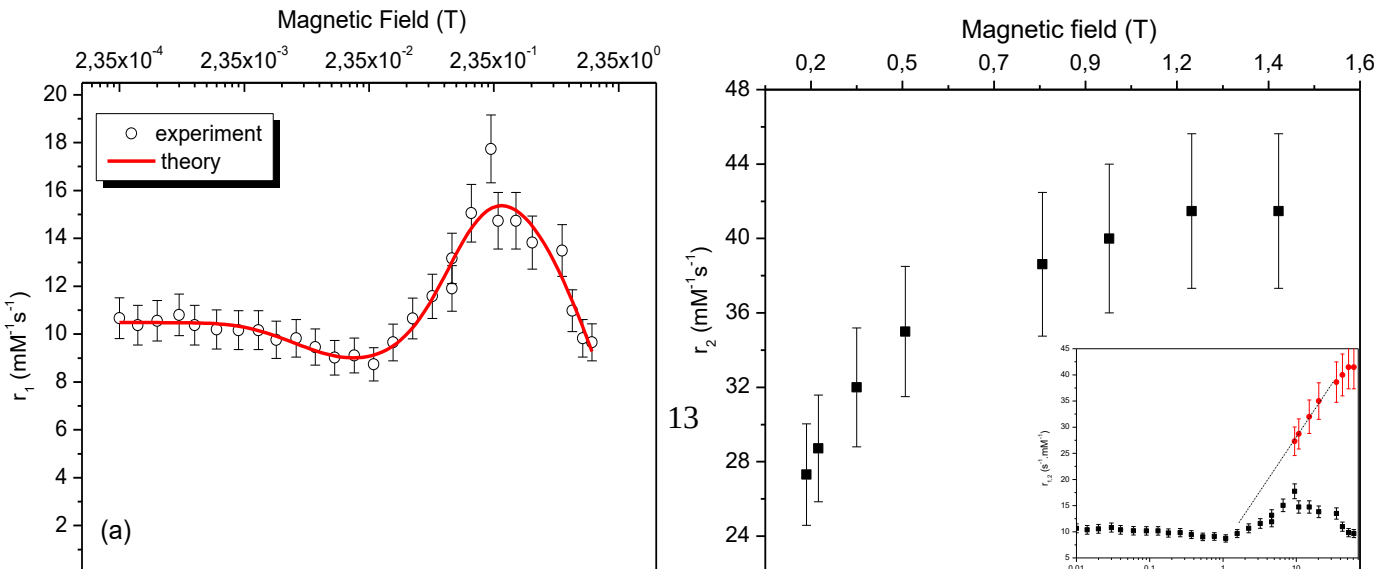

(b)

Fig.7. Frequency/field dependence of longitudinal (a) and transverse (b) relaxivity of water protons in $NiFe_2O_4$ nanoparticle suspension. Fitting of r_1-NMRD curve with theoretical model (Eq. 9) is also given in Fig.7a.

This behaviour is explained with theoretical model introduced by Roch et al.[50], which takes into account two mechanisms responsible for enhanced proton relaxation. The first mechanism is the afore-mentioned Néel reversal of particle magnetization characterized by τ_N (given in Eq.1). The second mechanism, the so-called "Curie relaxation", involves the Langevin function (Eq.2), representing the progressively aligning of magnetic moments in the field direction and the diffusion of water protons in the "outer sphere" of particle. This motion is characterized by a correlation time $\tau_D = R^2/D$, where R is the particle radius including the thickness of the organic coating (if impermeable to diffusing protons) and D is the diffusion coefficient of water. Since the Néel relaxation time τ_N depends on the anisotropy energy barrier, NMRD profile is also sensitive to particle's magnetic anisotropy; actually the local minima observed at Larmor frequency $\omega_I \approx 1$ MHz is due to the relatively low anisotropy of $NiFe_2O_4$ particles. This feature is typical for USPIO (Ultra Small Particle of Iron Oxide) with sizes d ≤ 4-5 nm and disappears for larger particles, in which the high anisotropy locks the particle magnetization along the easy-axis direction. From theoretical point of view, the frequency dependence of the two mechanisms contributing to the longitudinal nuclear relaxation is represented by Freed and Ayant spectral density functions, $J_F(\omega_I, \tau_D, \tau_N)$ and $J_A(\omega_I, \tau_D)$ respectively [51,52].The Roch's heuristic model linearly combines these functions with weighting parameters P and Q, whose values depend also on the anisotropy energy barrier of the particle. The complete equation describing the longitudinal relaxation rate is [53]:

$$r_1 = \left(\frac{32\pi}{135000}\right)\mu_{SP}^{*2}\gamma_I^2\left(\frac{N_A C}{RD}\right)\times\{7P\frac{L(x)}{x}J_F(\omega_I,\tau_D,\tau_N) + \left[7Q\frac{L(x)}{x} + 3(P+Q)\left(1 - L^2(x) - 2\frac{L(x)}{x}\right)\right]\times J_F(\omega_I,\tau_D,\tau_N) + 3L^2(x)J_A(\omega_I,\tau_D)\} \quad (9)$$

In Eq.9, μ_{SP}^* is the nanoparticle moment sensed locally by protons equal to $\mu_{SP}^* = AM_S V\rho$, where M_S is the saturation magnetization, V is the particle volume, ρ is the mass density of particle and A is an adjustment coefficient. Among other parameters, $\gamma_I$is the proton gyromagnetic ratio, R and D are, respectively, the minimum approach distance from particle center and the self-diffusion coefficient of water ($D=2.9\times10^{-5}cm^2.s^{-1}$), N_A is Avogadro's number, C is the molar concentration of nanoparticle and *L(x)* is the Langevin function given by Eq.2, where $x = \mu_{SP}^* H_0/k_B T$. Based on the results of TEM and magnetometry measurements giving intervals for R and M_S respectively, and setting τ_N as a free parameter (in addition to A and P=1-Q) the relaxation data given in Fig.7a were fitted with Eq.9. Table.2 gives the output values of these parameters together with the experimental values deduced from magnetic and structural characterization.

Table 2. Output parameters obtained by NMRD fitting and comparison with the values deduced from SQUID magnetometry and DLS experiments. The weighting parameters used in Eq.9 are A=0.93, P=0.28 and Q=0.72.

	Particle size $d_{NMR}=2R$ (nm)	Neel relaxation time τ_N (s)	Saturation magnetization M_S (emu/g)
NMR-D fitting	9.36	$2.57\text{x}10^{-9}$	39.9
Magnetometry and DLS	15	$2.3\text{x}10^{-9}$	40.8

As seen from Table.2, the calculated distance of minimum approach for protons as $d_{NMR}=2R$ is lower than the hydrodynamic diameter d_H obtained by DLS measurements: this is expected because, despite the organic coating prevents water molecules to diffuse closer to magnetic core center, they are able to penetrate the coating layer to some extent, making the d_{NMR} value smaller than hydrodynamic size (d_H), but larger than the magnetic core size (d_{TEM}). On the other hand, the values of Néel relaxation time τ_N and the saturation magnetization M_S are in good agreement with the ones deduced from magnetization measurements.

Besides valuable information included in longitudinal relaxivity r_1, transverse relaxivity r_2 has greater importance, since it is the fundamental parameter determining the MRI contrast enhancement efficiency of a superparamagnetic material. In Fig7b the increasing behavior of r_2 with frequency is an effect induced by particle magnetization, where the relaxivity is associated with the saturation degree of particles' magnetic moments in the corresponding magnetic field values (see Fig.4b) [1]. The observed r_2 profile is also explained by Roch's model, which predicts that for low frequencies (i.e. ω<1 MHz) r_1 and r_2 values should be equal. Based on the model we can tentatively expect that the increase in r_2 curve is further enhanced by the presence of particle agglomerates. Considering the entire agglomerate as a large magnetized sphere whose global magnetization is basically the sum of all individual particle moments forming the aggregate, the additional effect of the water proton diffusion around the whole aggregate characterized by a long correlation time τ_D, is the main reason of r_2 enhancement [54]. On the contrary, for the whole frequency range r_1 is diminished by the particle agglomeration based on a quite different mechanism called water exchange, which can be interpreted as the transfer of proton relaxation due to an exchange between the water molecules inside the agglomerates, rapidly relaxed, and the ones within the bulk, relaxing much slower [55]. As a result, at high magnetic fields the ratio r_2 / r_1, which is the real identifying quantity of the efficiency of a T_2-relaxing agent, increases depending on the magnetization state of the entire particle i.e. the concentration of nanoparticles in the agglomerate and the agglomerate size. Nevertheless, despite its relatively low transverse relaxivity, the as-prepared $NiFe_2O_4$ suspension shows a ratio r_2/ r_1 = 4.3. at 60 MHz proton Larmor frequency corresponding to 1.5 T, which is the magnetic field mostly used in MRI scanners. When compared with the accepted threshold value of r_2 / r_1 = 2 for an effective T_2-relaxing agent, the measured value implies that prepared $NiFe_2O_4$ nanoparticle suspension can be regarded as efficient negative contrast agent in MRI.

IV. CONCLUSIONS

We investigated the MRI contrast enhancement and hyperthermic properties of $NiFe_2O_4$ nanoparticles for potential use in diagnostic and therapeutic applications. Nanoparticles were synthesized with a modified co-precipitation method, where the probable toxic effect of nickel is hindered by post-synthetic coating of inorganic core with oleic acid and TMAH, the latter also acting as stabilizer ensuring non-precipitating particle dispersion in water. Characterization with XRD, TEM and HRTEM showed that the synthesized particles have single crystal nature and are nearly monodispersed with d=4.4 nm mean diameter

of the magnetic core and σ=3% standard deviation, whereas DLS measurements reveal that the hydrodynamic size is d_H≅15 nm and larger agglomerates, that in weak abundance, coexist with single particles in the aqueous suspension. The as-prepared sample possessed typical behavior of an ensemble of single domain superparamagnetic particles with ZFC-FC thermal irreversibility and blocking temperature, which can be described by Neel-Brown mechanisms. However the observed minor hysteresis imply that the agglomerated particles, which present more significant dipolar and/or exchange interactions than the isolated ones, are still in blocked regime at room temperature. Regarding the hyperthermic performance of $NiFe_2O_4$ nanoparticles, from ac-field induced temperature rise characteristics we obtained SAR values between 4 and 11 W/g for field intensities in the range H_0=17.2-23.7 kA/m and frequency f=170 kHz, where these field parameters are under human tolerable limits. These experimental SAR values were explained with observed hysteresis originated from agglomerated particles in ferromagnetic regime, whereas the estimations by applying LRT based model indicated that the mean size of isolated particles is too small to produce significant amount of heat through superparamagnetic relaxation. In calorimetric measurements a maximum temperature difference of ΔT=7 ºC was reached, meaning that starting from physiological temperatures local values of 42-45 ºC could be attained, a range of temperature at which the necrosis of tumor cells begins. On the other hand, longitudinal and transverse NMRD profiles have been obtained, where the experimental NMRD data were successfully fitted by employing the Roch model. The fitting procedure allowed us to determine the relative weights of Néel and Curie contributions to proton relaxation and to extract some important magnetic parameters which are in good agreement with magnetometry measurement results. It has been shown that, as the similar case in hyperthermia, the agglomeration affects the nuclear relaxation. The transverse relaxivity r_2 is increased due to the presence of agglomerates, since the water protons diffusing in the proximity of these large agglomerates experience relatively strong dipolar fields, depending on the intra-aggregate volume fraction of particles and the magnetization value. As a conclusion, the as-prepared $NiFe_2O_4$ nanoparticles can be regarded as promising theranostic agents to be simultaneously used for MRI diagnostics and MFH therapeutic purposes in nanomedicine.

ACKNOWLEDGMENTS

Prof. Alessandro Lascialfari (University of Pavia, Italy) is gratefully acknowledged for organizing SQUID and NMRD measurements and valuable contributions. We also thank to Prof. Tezer Fırat for the preparation of hyperthermia experiment setup, measurements and valuable discussions. Financial support from the University of Pisa though Progetti di Ricerca di Ateneo (grant PRA_2017_25).

REFERENCES

[1] Martina, M. S., Fortin, J. P., Menager, C., Clement, O., Barratt, G., Grabielle-Madelmont, C., Gazeau, F., Cabuil, V and Lesieur, S., Generation of Superparamagnetic Liposomes Revealed as Highly Efficient MRI Contrast Agents for in Vivo Imaging, Journal of American Chemical Society, 2005, 127, pp.10676-10685

[2] Li,L., Jiang, W., Luo, K., Song, H., Lan, F., Wu,Y.,Gu, Z., Superparamagnetic Iron Oxide Nanoparticles as MRI contrast agents for Non-invasive Stem Cell Labeling and Tracking, Theranostics, 2013, 3 (8), pp.595-615

[3] Umut, E., Pineider, F., Arosio, P., Sangregorio, C., Corti, M., Tabak, F., Lascialfari, A.,Ghigna, P., Magnetic, Optical and Relaxometric Properties of Organically CoatedGold-magnetite (Au-Fe3O4) Hybrid Nanoparticles for Potential use in Biomedical Applications,Journal of Magnetism and Magnetic Materials, 2012, 324, pp. 2373-2379

[4] Gossuin, Y., Gillis, P., Hocq, A., Vuong, Q. L. and Roch, A., Magnetic Resonance RelaxationProperties of Superparamagnetic Particles, WIREs Nanomedicine and Nanobiotechnology,2009, 1, pp. 299-310

[5] Kim, D. H., Nikles, D. E., Johnson, D. T., Brazel, C. S., Heat Generation of Aqueously Dispersed $CoFe_2O_4$ Nanoparticles as Heating Agents for Magnetically ActivatedDrug Delivery and Hyperthermia, Journal of Magnetism and Magnetic Materials,2008, 320 (19), pp.2390–2396

[6] Gonzales, M., and Krishnan, K. M., Synthesis of Magnetoliposomes with Monodisperse Iron oxide Nanocrystal Cores for Hyperthermia, Journal of Magnetism and Magnetic Materials, 2005, 293 (1), pp.265–270

[7] Hergt, R. and Dutz, S., Magnetic Particle Hyperthermia-Biophysical Limitations of a Visionary Tumor Therapy, Journal of Magnetism and Magnetic Materials, 2007, 311 (1), pp.187-192

[8] Barick, K. C., Singh, S., Bahadur, D., Lawande, M. A., Patkar, D. P., Hassan, P. A., Carboxyl decorated Fe_3O_4 nanoparticles for MRI diagnosis and localized hyperthermia, Journal of Colloid and Interface Science, 2014, 418, pp.120-125

[9] Jiang, Q. L., Zheng, S. W., Hong, R. Y., Deng, S. M., Guo, L., Hu, R. L., Gao, B., Huang, M., Cheng, L. F., Liu, G. H., Wang, Y. Q., Folic acid-conjugated Fe_3O_4 magnetic nanoparticles for hyperthermia and MRI in vitro and in vivo, Applied Surface Science, 2014, 307, pp.224-233

[10] Yin, H., Too, H. P. and Chow, G. M., The effects of particle size and surface coating on the cytotoxicity of nickel ferrite, Biomaterials, 2005, 26, pp.5818-5826

[11] Rana, S., Gallo, A., Srivastava, R. S. and Misra, R. D. K., On the suitability of nanocrystalline ferrites as a magnetic carrier for drug delivery: Functionalization, conjugation and drug release kinetics, Acta Biomateriala, 2007, 3, pp.233-242

[12] Nathani, H., Gubbala, S. and Misra, R. D. K., Magnetic behavior of nickel ferrite-polyethylene nanocomposites synthesized by mechanical milling process, Materials Science and Engineering B, 2004, 111, pp.95-100

[13] Sepelak, V., Baabe, D., Mienert, D., Schultze, D., Krumeich, F., Litterst, F. J., Becker, K. D., Evolution of structure and magnetic properties withannealingtemperature in nanoscale high-energy-milled nickel ferrite, Journal of Magnetism and Magnetic Materials, 2003, 257, pp.377-386

[14] Sepelak, V., Bergmann, I., Feldhoff, A., Heitjans, P., Krumeich, Menzel, D., F., Litterst, F. J., Campbell, S. J., Becker, K. D., Nanocrystalline Nickel Ferrite, $NiFe_2O_4$: Mechanosynthesis, Nonequilibrium Cation Distribution, Canted Spin Arrangement, and Magnetic Behavior, Journal of Physical Chemistry C, 2007, 111, pp. 5026-5033

[15] Nawale, A. B., Kanhe, N. S., Patil, K. R., Bhoraskar, S. V., Mathe, V. L., Das, A. K., Magnetic properties of thermal plasma synthesized nanocrystalline nickel ferrite ($NiFe_2O_4$), Journal of Alloys and Compounds, 2011, 509, pp.4404-4413

[16] Srivastava, M., Chaubey, S. And Ojha, A. K., Investigation on size dependent structural and magnetic behavior of nickel ferrite nanoparticles prepared by sol–gel and hydrothermal methods, Materials Chemistry and Physics, 2009,118, pp.174-180

[17] Maaz, K., Karim, S., Mumtaz, A., Hasanain, S. K., Liu, J., Duan, J. L., Synthesis and magnetic characterization of nickel ferrite nanoparticles prepared by co-precipitation route, Journal of Magnetism and Magnetic Materials, 2009, 321, 1838-1842

[18] Jacob, J. and Khadar, M. A.,Investigation of mixed spinel structure of nanostructured nickel ferrite, Journal of Applied Physics, 2010, 107, pp.114310

[19] Chen, D., Chen, D., Jiao, X., Zhao, Y., He, M., Hydrothermal synthesis and characterization of octahedral nickelferrite particles, Powder Technology, 2003, 133, pp.247-250

[20] Kale, A., Gubbala, S. and Misra, R. D. K., Magnetic behaviour of nanocrystalline nickel ferrite synthesized by the reverse micelle technique, Journal of Magnetism and Magnetic Materials, 2004, 277, pp.350-358

[21] Shultz, M. D., Scott, C., Fatouros P. P., Morrison, S. A., Carpenter, E. E., Enhanced ferrite nanoparticles as MRI contrast agents, Journal of Magnetism and Magnetic Materials, 2007, 311, pp.464-468

[22] Bae, S. and Lee, S. W.,Applications of $NiFe_2O_4$ nanoparticles for a hyperthermia agent in biomedicine, Applied Physics Letters, 2006, 89, pp.252503

[23] Bae, S., Lee, S. W., Hirukawa, A., Takemura, Y., Jo, Y. H., Lee, S. G., AC magnetic field induced heating and physical properties of ferrite nanoparticles for a hyperthermia agent in medicine, IEEE Transactions on Nanotechnology, 2009, 8 (1), pp.86-94

[24] Caruntu, D., Remond, Y., Chou, N. H., Jun, M. J., Caruntu, G., He, J.B., Goloverda, G., O'Connor, C., Kolesnichenko, V.,Reactivity of 3D transition metal cations in diethylene glycol solutions. Synthesis of transition metal ferrites with the structure of discrete nanoparticles complexed with longchain carboxylate anions. Inorganic Chemistry, 2002, 41, pp.6137–6146

[25] S. W. Provencher, A constrained regularization method for inverting data represented by linear algebraic or integral equations, Computer Physics Communication, 1982, 27 (3), pp.213-227

[26] Hasmonay, E., Depeyrot, J., Sousa, M. H., Tourinho, F. A., Bacri, J. C., Perzynski, R., Raikher, Y. L., Rosenman, I., Magnetic and optical properties of ionic ferrofluids based on nickel ferrite nanoparticles, Journal of Applied Physics, 2000, 88, pp.6628-6635

[27] Li, X., Tan, G., Chen, W., Zhou, B., Xue, D., Peng, Y., Li, F., Mellors, N. J., Nanostructural and magnetic studies of virtually monodispersed $NiFe_2O_4$ nanocrystals synthesized by aliquid-solid-solution assisted hydrothermal route, 2012, Journal of Nanoparticle Research, 14:751

[28] Neél, L., Thermoremanent Magnetization of Fine Powders, Reviews of Modern Physics, 1953, 25 (1), pp.293-295

[29] Dormann, J. L., Bessais, L. and Fiorani, D, 1988, A dynamic study of small interacting particles: superparamagnetic model and spin-glass laws, Journal of Physics C, 21, 10, 2015-2034.

[30] Skomski, R., Nanomagnetics, Journal of Physics: Condensed Matter, 2003, 15 (20), pp.841-896

[31] Kodama, R. H., Berkowitz, A. E., McNiff, E. J., Foner, S., Surface spin disorder in $NiFe_2O_4$ Nanoparticles, Physical Review Letters, 1996, 77 (2), 394-397

[32] Hergt, R., Dutz, S., Müller, R., Zeisberger, M., Magnetic particle hyperthermia: nanoparticle magnetism and materials development for cancer therapy, Journal of Physics: Condensed Matter, 2006, 18, pp.2919-2934

[33] Hergt, R., Dutz, S., Röder, M., Effects of size distribution on hysteresis losses of magnetic nanoparticles for hyperthermia, Journal of Physics: Condensed Matter, 2008, 20, 385214 (12pp)

[34] Bae, S., Lee, S. W., Hirukawa, A., Takemura, Y., Jo, Y. H., Lee, S. G., AC magnetic-field-induced heating and physical properties of ferrit nanoparticles for a hyperthermia agent in medicine, IEEE Transactions on Nanotechnology, 2009, 8 (1), pp.86-94

[35] Atkinson, W. J.; Brezovich, I. A.; Chakraborty, D. P. IEEE Transactions: Biomedical Engineering, 1984, 31, 70.

[36] Landau, L. D., Lifshitz, E. M., Electrodymanics of Continous Media, Pergamon Press, London, 1960

[37] Rosenweig, R. E., Heating magnetic fluid with alternating magnetic field, Journal of Magnetism and Magnetic Materials, 2002, 252, pp.370-374

[38] Yelenich, O. V., Solopan, S. O., Kolodiazhnyi, T. V., Dzyublyuk, V. V., Tovstolytkin, A. I., Belous, A. G., Superparamagnetic behavior and ac-losses in $NiFe_2O_4$ nanoparticles, Solid State Sciences, 2013, 20, pp.115-119

[39] Eggeman, A. S., Majetich, S. A., Farrell, D., Pankhurst, Q. A., Size and concentration effects on high frequency hysteresis of iron oxide nanoparticles, IEEE Transactions on Magnetics, 2007, 43(6), pp.2451-2453

[40] Jeun, M., Bae, S., Tomitaka, A., Takemura, Y., Park, K. H., Paek, S. H., Chung, K. W., Effects of particle dipole interaction on the ac magnetically induced heating characteristics of ferrite nanoparticles for hyperthermia, Applied Physics Letters, 2009, 95, 082501-3

[41] Dennis, C. L., Jackson, A. J., Borchers, J. A., Hoopes, P. J., Strawbridge, R., Foreman, A. R., Lierop, J., Grüttner, C., Ivkov, R., Nearly complete regression of tumors via collective behavior of magnetic nanoparticles in hyperthermia, Nanotechnology, 2009, 20, 395103-7

[42] Yuan, Y. and Borca-Tasciuc, D., Anomalously high specific absorption rate in bioaffine ligand-coated iron oxide nanoparticle suspensions, IEEE Transactions on Magnetics, 2013, 49, pp.263-8

[43] Boubeta-Martinez, C., Simeonidis, K., Makridis, A., Angelakeris, M., Iglesias, O., Guardia, P., Cabot, A., Yedra, L., Estrade, S., Peiro, F., Saghi, Z., Midgley, P. A., Leboran-Conde, I., Serantes, D., Baldomir, D., Learning from Nature to Improve the Heat Generation of Iron-Oxide Nanoparticles for Magnetic Hyperthermia Applications, Nature Scientific Reports, 2012, 3, 1652

[44] Landi, G. T., Role of dipolar interaction in magnetic hyperthermia, Physical Review B, 2014, 89, 014403

[45] Mehdaoui, B., Tan, R. P., Meffre, A., Carrey, J., Lachaize, S., Chaudret, B., Respaud, M., Increase of magnetic hyperthermia efficiency due to dipolar interactions in low-anisotropy magnetic nanoparticles: Theoretical and experimental results, Physical Review B, 2013, 87, 174419

[46] Lima, E. J., Biasi, E. D., Mansilla, M. V., Saleta, M. E., Granada, M., Troiani, H. E., Effenberger, F. B., Rossi, L. M., Rechenberg, H. R., Zysler, R. D., Heat generation in agglomerated ferrite nanoparticles in an alternating magnetic field, Journal of Physics D: Applied Physics, 2013, 46, 045002

[47] Singh, V. And Banerjee, V., Ferromagnetism, hysteresis and enhanced heat dissipation in assemblies of superparamagnetic nanoparticles, Journal of Applied Physics, 2012, 112, 114912

[48] Serantes, D.,Baldomir, D., Martinez-Boubeta, C., Simeonidis, K., Angelakeris, M., Natividad, E., Castro, M., Mediano, A., Chen, D. X., Sanchez, A., Balcells, LI, Martínez, B., Influence of dipolar interactions on hyperthermia properties of ferromagnetic particles, Journal of Applied Physics, 2010, 108, 073918

[49] Haase, C. and Nowak, U., Role of dipole-dipole interactions for hyperthermia heating of magnetic nanoparticle ensembles, Physical Review B., 2012, 85, 045435

[50] Roch, A., Muller, R. N., Gillis, P., Theory of proton relaxation induced by superparamagnetic particles, Journal of Chemical Physics, 1999, 110, pp. 5403-5411

[51] Freed, J. H., Dynamic effects of pair correlation functions on spin relaxation by translational diffusion in liquids. II. Finite jumps and independent T_1 processes, Journal of Chemical Physics, 1978, 68, 4034

[52] Ayant, Y., Belorizky, E., Alizon, J. and Galice, J., 1975, Calcul des densités spectrales résultant d'un mouvement aléatoire de translation en relaxation par interaction dipolaire magnétique dans les liquides, Journal de Physique, 36, 991.

[53] Bordonali, L., Kalaivani, T., Sabareesh, K. P. V., Innocenti, C., Fantechi, E., Sangregorio, C., Casula, M. F., Lartigue, L., Larionova, J., Guari, Y., Corti, M., Arosio, P., Lascialfari, A., NMR-D study of the local spin dynamics and magnetic anisotropy in different nearly monodispersed ferrite nanoparticles, Journal of Physics: Condensed Matter, 2013, 25, 066008

[54] Laurent, A., Nicotra, C., Gossuin, Y., Roch, A., Ouakssim, A., Vander Elst, A., Cornant, M., Soleil, P., Muller, R. N., Influence of the length of the coating molecules on the nuclear magnetic relaxivity of superparamagnetic colloids, Physical Status Solidi C, 2004, 1, 12, pp. 3644-3650

[55] Roch, A., Gossuin, Y., Muller, R. N., Gillis, P., Superparamagnetic colloid suspensions: Water magnetic relaxation and clustering, Journal of Magnetism and Magnetic Materials, 2005, 293, pp. 532-539